Coulomb-Volkov approximation for near-threshold ionization by short laser pulses

Diego G. Arbó, Jorge E. Miraglia, and María Silvia Gravielle
Institute for Astronomy and Space Physics, IAFE, CC 67, Suc. 28 (1428), Buenos Aires, Argentina
and Department of Physics, FCEN, University of Buenos Aires, Buenos Aires, Argentina

Klaus Schiessl, Emil Persson, and Joachim Burgdörfer
Institute for Theoretical Physics, Vienna University of Technology, Wiedner Hauptstrasse 8-10/136, A-1040 Vienna, Austria
(Received 22 June 2007; published 8 January 2008)

The formation of near-threshold structures in the angle-resolved photoelectron spectrum, the cusp in the transverse electron momentum distribution, and the forward-backward asymmetry is influenced by the residual Coulomb potential of the remaining atomic core acting on the electron detached by strong short-laser pulses. We show that an improvement beyond the strong-field approximation—the Coulomb-Volkov distorted wave approximation—is capable to reproduce these features found in the exact solution of the time-dependent Schrödinger equation in the multiphoton regime and the transition from the multiphoton to the tunneling regime.

DOI: 10.1103/PhysRevA.77.013401 PACS number(s): 32.80.Rm, 32.80.Fb, 03.65.Sq

I. INTRODUCTION

Recent advances in laser technology have resulted in the availability of intense, phase-stabilized and phase-controlled few-cycle infrared laser pulses [1]. The interaction of such short and strong pulses with matter is a topic which has attracted much interest recently. Many experimental (see, for example, [2,3]) and theoretical studies have been performed along these lines. Calculations employ different methods: *ab initio* solutions of the time-dependent Schrödinger equation (TDSE) [4,5], quantum methods of different degrees of approximation, such as the first Born and the strong-field approximations (SFA) [6–12], and quasiclassical trajectory Monte Carlo methods, where Hamilton's equations of motion are solved by means of a classical trajectory Monte Carlo approach that includes tunneling (CTMC-T) [13,14].

Stringent tests of the theory became possible with the advent of the COLTRIMS technique, which allows the imaging of the vectorial momentum distribution of the reaction fragments. A recently measured [15,16] complex emission pattern near threshold in the two-dimensional momentum plane—parallel and perpendicular to the laser polarization axis—for rare-gas atoms revealed diffraction oscillations as a result of the interference of classical paths of electrons released at different times but reaching the same Kepler asymptote in the Coulomb field [17]. For the case of single photodetachment from negative ions, i.e., H^-, near-threshold angular distributions were intuitively explained with a double-slit interference model [18–21].

Another test of ionization theories is provided by the momentum distribution transverse to the polarization axis since the (nonrelativistic) electric field of the laser does not transfer momentum in this direction to leading order. First experiments [22] were in accord with a smooth Gaussian transverse distribution predicted by the tunneling theory of Delone and Krainov (DK), which treats Coulomb interactions as a weak perturbation [23]. Methods involving the SFA also exhibit a Gaussian-like transverse momentum distribution [14,23,24]. However, recent high-resolution experiments for single ionization of rare-gas atoms [25] showed spectra exhibiting a sharp cusplike structure around zero transverse momentum, differing from the DK or SFA predictions. Quasiclassical CTMC-T simulations reproduce the cusp shape when the Coulomb interaction of the active electron with its parent ion is taken into account [14]. In contrast, when the Coulomb interaction is neglected after tunneling, a Gaussian distribution is recovered in accordance with the DK theory.

A few years ago Paulus *et al.* [26] found a right-left (also called forward-backward) asymmetry of photoelectron spectra produced by short laser pulses. Several theoretical works [27–29] have addressed this topic. By means of a classical model Chelkowski and Bandrauk [28] showed that the Coulomb attraction by the remaining core is responsible for such an asymmetry for pulses with a cosinelike envelope. Chen *et al.* [24] studied the importance of the long-range Coulomb interaction and showed that calculations based on the SFA fail to properly reproduce both the correct shape pattern near the threshold in the doubly-differential momentum distribution and the cusp at origin in the transversal momentum distribution. Inclusion of Coulomb effects into the final state was found to be important for total ionization rates and photoelectron spectra [30].

In the present work we study the performance of the Coulomb-Volkov distorted-wave approximation (CVA) to describe the complex near-threshold energy region of photoemission spectra. The CVA is a time-dependent distorted-wave theory [9,10] that allows to include into the final state the effect of the remaining core at the same level of approximation as the laser field. In this way, we can directly probe the effect of the core potential on the dynamics of the detached electron. We employ the CVA to determine the near-threshold emission pattern, the transversal cusp, and the forward-backward asymmetry for a few-cycle linearly polarized laser field. Results are compared with values derived from the SFA and with full numerical results of the TDSE [17,31], which can be considered as the exact solution. We show that the inclusion of the Coulomb potential within the CVA leads to the appearance of near threshold bouquet-shape patterns in doubly-differential momentum distributions and the formation of the cusp in transverse momentum distribu-

tions. Much of the forward-backward asymmetry of the measured distributions can be accounted for. Furthermore, by selectively switching-off certain contributions of the distortion produced by the residual ion, their relative importance can be assessed. For example, the reduction of the Coulomb effect to a multiplicative preexponential factor [32], while improving the absolute emission rate, does not improve the two-dimensional distribution pattern.

In Sec. II we summarize the different levels of the time-dependent distorted-wave theory: (i) the well-known Volkov (V), Keldysh-Faisal-Reiss or strong-field approximations [33], and (ii) the CVA, which includes the influence of the atomic core on the ejected electron [9,10,34]. We also briefly describe the *ab initio* method to solve the time-dependent Schrödinger equation and the projection onto outgoing Coulomb states with well-defined asymptotic momenta. In Sec. III we discuss results for the formation of the low-energy structures in the doubly-differential electron momentum distributions, the appearance of the cusp in the transverse momentum distribution, and the carrier-envelope phase dependence of the forward-backward asymmetry of the longitudinal distribution. Atomic units (a.u.) are used throughout.

II. THEORY

We consider the interaction of a target atom with an ultrashort laser pulse, which is described through a time-dependent electric field along the $\hat{\mathbf{z}}$ direction. The field $\mathbf{F}(t)$ reads

$$\mathbf{F}(t) = f(t)\cos(\omega t + \phi_{\mathrm{CE}})\hat{\mathbf{z}}, \tag{1}$$

where ω is the laser frequency, ϕ_{CE} the relative carrier-envelope phase, and $f(t)$ is the envelope function of the pulse,

$$f(t) = \begin{cases} F_0 \cos^2\left(\dfrac{\pi t}{\tau}\right) & \text{for } -\tau/2 \le t \le \tau/2, \\ 0 & \text{otherwise,} \end{cases} \tag{2}$$

with total duration τ. As a consequence of the interaction, one electron initially bound to the target nucleus in the state $|\phi_i\rangle$ is emitted with momentum $\mathbf{k}$ and energy $\varepsilon_f = k^2/2$ upon conclusion of the pulse into the final unperturbed state $|\phi_f\rangle$, where $k = |\mathbf{k}|$. The evolution of the electronic state $|\psi(t)\rangle$ is governed by the time-dependent Schrödinger equation for the Hamiltonian $H(t) = H_0 + V(t)$, where H_0 is the atomic Hamiltonian and $V(t) = \mathbf{r}\cdot\mathbf{F}(t)$ is the interaction with the laser field in the length gauge.

We confine our study to a hydrogen atom initially in its ground state. Thus, the process possesses cylindrical symmetry around the polarization axis and the azimuthal angle is cyclic. Electron momentum distributions can be calculated from the transition matrix as

$$\frac{dP}{d\mathbf{k}} = |T_{if}|^2, \tag{3}$$

where T_{if} is the T-matrix element corresponding to the transition $\phi_i \to \phi_f$. In this work, T_{if} will be computed using three different methods, namely (i) the SFA; (ii) the CVA; and (iii) the numerical solution of the TDSE, considered to be the exact solution and used as a benchmark for assessing the reliability of the previous approximations. We also discuss the eikonal-Volkov approximation (EVA), which is a variant of the CVA.

A. Time-dependent distorted-wave methods

Within the time-dependent distorted wave theory [35], the transition amplitude in the *post* form is expressed as

$$T_{if} = -i\int_{-\infty}^{+\infty} dt \langle \chi_f^-(t)|V(t)|\phi_i(t)\rangle, \tag{4}$$

where $\chi_f^-(t)$ is the final distorted-wave function. In the present case

$$i\frac{\partial}{\partial t}|\phi_i(t)\rangle = H_0|\phi_i(t)\rangle = \left(\frac{p^2}{2} + V_C\right)|\phi_i\rangle = \varepsilon_i|\phi_i\rangle, \tag{5}$$

where V_C is the atomic core potential.

Different distorted-wave approximations result from different choices of the distortion potential to be included in $|\chi_f^-\rangle$:

(a) Choosing identical Hamiltonians for the entrance-channel Hamiltonian and exit-channel distorted Hamiltonian, $|\chi_f^-\rangle = |\phi_{\mathbf{k}}^-\rangle$, which corresponds to

$$H_f|\chi_f^-\rangle = H_0|\phi_{\mathbf{k}}^-\rangle = \varepsilon_f|\phi_{\mathbf{k}}^-\rangle. \tag{6}$$

In this case, Eq. (4) reduces the first Born approximation, which is clearly insufficient in the strong-field regime. In Eq. (6), $\phi_{\mathbf{k}}^-$ is the unperturbed final state given by

$$\phi_{\mathbf{k}}^-(\mathbf{r}) = e^{-i\varepsilon_f t}\frac{\exp(i\mathbf{k}\cdot\mathbf{r})}{(2\pi)^{3/2}}\mathcal{D}_C(Z_T,\mathbf{k},t), \tag{7}$$

where $\mathcal{D}_C(Z_T,\mathbf{k},t) = N_T^-(k)\ {}_1F_1(-iZ_T/k,1,-ik\ r - i\mathbf{k}\cdot\mathbf{r})$. The Coulomb normalization factor $N_T^-(k) = \exp(\pi Z_T/2k)\Gamma(1 + iZ_T/k)$ coincides with the value of the Coulomb wave function at the origin, ${}_1F_1$ denotes the confluent hypergeometric function, Z_T is the electric charge of the parent ion.

(b) Choosing the Hamiltonian of a free electron in the time-dependent electric field as the exit-channel distorted Hamiltonian,

$$i\frac{\partial}{\partial t}|\chi_f^-(t)\rangle = H_f|\chi_f^-(t)\rangle = \left(\frac{p^2}{2} + V(t)\right)|\chi_f^-(t)\rangle. \tag{8}$$

The solutions are the Volkov states [36]

$$\chi_{\mathbf{k}}^{(V)-}(\mathbf{r},t) = \frac{\exp(i\mathbf{k}\cdot\mathbf{r})}{(2\pi)^{3/2}}e^{-i\varepsilon t}\exp[iD^-(\mathbf{k},\mathbf{r},t)], \tag{9}$$

with

$$D^-(\mathbf{k},\mathbf{r},t) = \mathbf{A}^-(t)\cdot\mathbf{r} - \mathbf{k}\cdot\int_{+\infty}^{t} dt'\mathbf{A}^-(t') - \frac{1}{2}\int_{+\infty}^{t} dt'[\mathbf{A}^-(t')]^2 \tag{10}$$

the so-called Volkov phase, and $\mathbf{A}^-(t') = -\int_{+\infty}^{t} dt'\ \mathbf{F}(t')$ the vector potential of the field multiplied by the speed of light. Inserting Eq. (9) into (4) leads to the SFA.

(c) Combining the final-channel wave functions of Eqs. (6) and (8) in a product form results in the Coulomb-Volkov final state [34]

$$\chi_{\mathbf{k}}^{(\mathrm{CV})-}(\mathbf{r},t) = \phi_{\mathbf{k}}^{-} \exp[iD^{-}(\mathbf{k},\mathbf{r},t)] = \chi_{\mathbf{k}}^{(V)-}(\mathbf{r},t)\mathcal{D}_C(Z_T,\mathbf{k},t). \tag{11}$$

Inserting the distorted wave function [Eq. (11)] into Eq. (4) we arrive at the CVA, which can be evaluated in a closed form [9,10]. Obviously, the two former approximations are limiting cases of Eq. (11). The Born approximation results from Eq. (11) in the limit $D^{-} \to 0$, while the SFA corresponds to the limit $Z_T \to 0$. The CVA, for laser-atom interactions first proposed by Jain and Tzoam [37], is a member of the class of approximations originally proposed by Cheshire [38] and Vainstein *et al.* [39] for ionizing charged particle collisions. There, the simultaneous Coulomb interactions of the released electron with the residual ionic core and the charged projectile are taken into account in terms of a product of two two-body Coulomb functions, which leads to a distorted wave function called the continuum-distorted wave (CDW). The CDW allows to include the effect of the two Coulomb fields non-perturbatively yet approximately.

(d) A further variant of a distorted wave approximation can be derived by invoking the asymptotic expansion of the Coulomb wave function for large arguments,

$$\mathcal{D}_C(Z_T,\mathbf{k},t) \underset{r\to\infty}{\to} \exp[iZ_T/k \ln(\mathbf{k}\cdot\mathbf{r} + kr)]. \tag{12}$$

This asymptotic approximation to the full Coulomb function corresponds to the inclusion of the Coulomb phase accumulated along straight-line trajectories, while neglecting deflections in the Coulomb field. This observation is of significance when applied to the near-threshold behavior of the strong-field ionization spectrum. Inserting Eq. (12) into Eqs. (11) and (4) leads to the eikonal-Volkov distorted wave approximation (EVA).

For the electric field of Eq. (1) with a carrier-envelope phase $\phi_{\mathrm{CE}}=0$, the vector potential fulfills the relation: $\mathbf{A}^{-}(t)=-\mathbf{A}^{-}(-t)$. Hence, the Volkov phase [Eq. (10)] fulfills $D^{-}(\mathbf{k},\mathbf{r},t)=-D^{-}(-\mathbf{k},\mathbf{r},\tau-t)$. Therefore, the final Volkov state behaves as

$$\chi_{\mathbf{k}}^{(V)-}(\mathbf{r},t) = \exp(-i\varepsilon_f\tau)[\chi_{-\mathbf{k}}^{(V)-}(\mathbf{r},\tau-t)]^{*}. \tag{13}$$

By inserting Eq. (13) into Eq. (4) and assuming the initial state to be of even parity, $\phi_i(\vec{r})=\phi_i(-\vec{r})$, it is easy to derive the following property for the transition amplitude in the SFA: $T_{if}^{\mathrm{SFA}}(\mathbf{k})=\exp[i(\varepsilon_f-\epsilon_i)\tau][T_{if}^{\mathrm{SFA}}(-\mathbf{k})]^{*}$. Consequently, the final momentum distribution is an even function in the longitudinal momentum,

$$\frac{dP(k_z)}{d\mathbf{k}} = \frac{dP(-k_z)}{d\mathbf{k}}. \tag{14}$$

This symmetry, which is an artifact of the SFA, is broken by the Coulomb distortion in the exit channel. The degree of forward-backward asymmetry is therefore a direct measure of the influence of the Coulomb field on the receding electron.

B. TDSE calculations

The time-dependent Schrödinger equation can be solved by means of the generalized pseudospectral method [5]. This method combines a discretization of the radial coordinate optimized for the Coulomb singularity with quadrature methods to achieve stable long-time evolution using a split-operator method. It allows for an accurate description of both the unbound as well as the bound parts of the wave function $|\psi(t)\rangle$. Emission of an electron with wave vector $\mathbf{k}$ is determined by the projection of the evolved wave packet onto Coulomb scattering states [4,40,41]. Therefore, after the laser pulse is turned off, the wave packet is projected onto outgoing Coulomb wave functions, which gives the transition amplitude

$$T_{i,\mathbf{k}} = \frac{1}{\sqrt{4\pi k}} \sum_l e^{i\delta_l(k)} \sqrt{2l+1} P_l(\cos\theta) \langle k,l \,|\psi(\tau)\rangle, \tag{15}$$

where $\delta_l(k)$ is the momentum-dependent Coulomb phase shift, θ is the angle between $\mathbf{k}$ and the polarization direction of the laser field (taken to be along $\hat{\mathbf{z}}$), P_l is the Legendre polynomial of degree l, and $|k,l\rangle$ is the eigenstate of the free atomic Hamiltonian with positive eigenenergy $\varepsilon=k^2/2$ and orbital quantum number l. The Coulomb projection is needed since $\mathbf{k}$ is not a constant of motion of the free evolution (once the external field is turned off) unlike the photoelectron energy spectrum, as the energy is a constant of motion of the free evolution.

III. RESULTS AND DISCUSSION

A. Structures in the two-dimensional electron momentum distribution

A detailed analysis of the electron yield for atomic ionization produced by an external laser field can be performed in terms of the doubly-differential momentum distribution. Time-dependent distorted-wave theories of Sec. II A provide us with an excellent tool to analyze the relative importance of the two competing fields, the optical and ionic Coulomb fields on the wave packet of the released electron.

We start with a laser pulse with a peak field $F_0=0.05$ a.u., frequency $\omega=0.25$ a.u., and total duration $\tau=151$ a.u., corresponding to six complete optical cycles. The resulting Keldysh parameter $\gamma=5$ indicates the dominance of the multiphoton process [$\gamma=(\omega/F_0)\sqrt{2I_p}$, where I_p is the ionization potential of the atom [33]]; at least two photons are needed to reach the continuum. Except in Sec. III C, we consider always cosinelike pulses (zero carrier-envelope phase, i.e., $\phi_{\mathrm{CE}}=0$). In Fig. 1, the doubly-differential momentum distribution, $d^2P/dk_\rho dk_z$, as a function of the final longitudinal (k_z) and transverse ($k_\rho=\sqrt{k_x^2+k_y^2}$) components of the electron momentum is shown. Both approximations reproduce [Figs. 1(a) and 1(b)] the overall above threshold ionization (ATI) ring pattern of the exact *ab initio* calculation [Fig. 1(c)]. However, the near-threshold bouquet structure, which results from the dominance of a single partial wave [17] [in the present case $l=2$, $\sim|Y_2^0(\theta)|^2$], is only reproduced by the CVA and not by SFA. Such failure of the SFA has also been observed in [24].

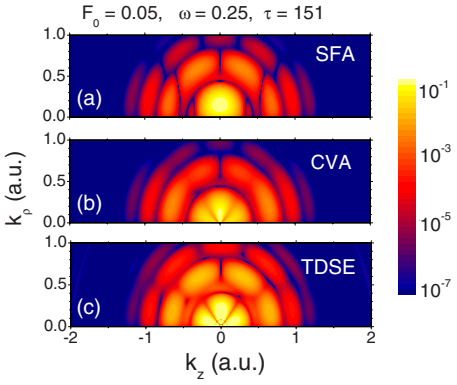

FIG. 1. (Color online) Doubly-differential electron momentum distributions (logarithmic scale) in cylindrical coordinates (k_z,k_ρ) using (a) the SFA, (b) the CVA, and (c) the exact TDSE calculation: The parameters of the field are $F_0=0.05$ a.u., $\omega=0.25$ a.u., and $\tau=151$ a.u. which comprises six complete optical cycles.

We now inquire into the relative importance of different contributions due to the Coulomb field, that is, the Coulomb normalization factor $N_T^-(k)$, which has been employed in the past as a correction factor to the SFA [33], and the Coulomb wave function factor ${}_1F_1$ [see Eq. (11)]. For this purpose we compare results obtained by including in $\mathcal{D}_C$ either only the Coulomb factor $N_T^-(k)$ [Fig. 2(a)] or only the hypergeometric function ${}_1F_1$ [Fig. 2(b)]. The distribution of Fig. 2(a) resembles very much the SFA distribution [Fig. 1(a)], which shows that the inclusion of the Coulomb factor $N_T^-(k)$ in the Coulomb-Volkov final function of Eq. (11) increases the total ionization probability (in the present case by a factor 2) but does not change the emission pattern near the threshold predicted by the SFA. This is to be expected since the Coulomb

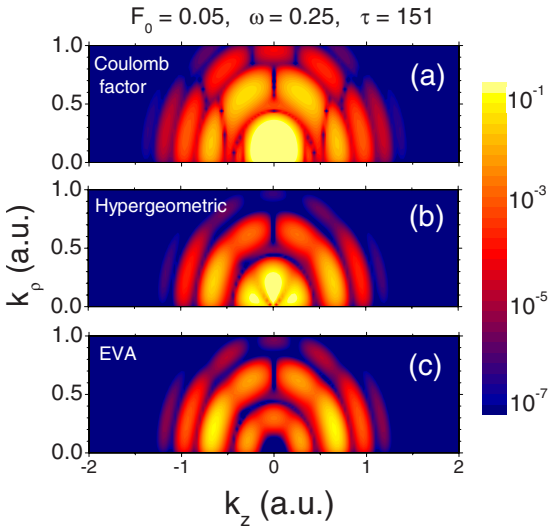

FIG. 2. (Color online) Doubly-differential electron momentum distributions (logarithmic scale) in cylindrical coordinates (k_z,k_ρ) using (a) only the Coulomb normalization factor $N_T(k)$ with the SFA, (b) only the hypergeometric function ${}_1F_1$ with the SFA [see Eq. (11)], and (c) the EVA [see Eq. (12)]. The parameters of the field are the same as in Fig. 1.

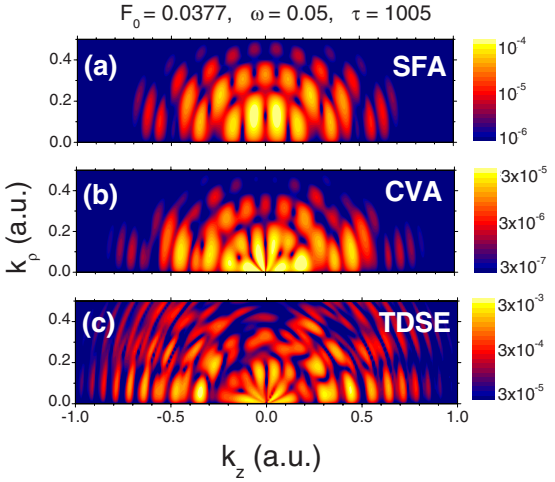

FIG. 3. (Color online) Doubly-differential electron momentum distributions (logarithmic scale) in cylindrical coordinates (k_z,k_ρ) using (a) the SFA, (b) the CVA, and (c) exact TDSE calculation: The parameters of the field are $F_0=0.0377$ a.u., $\omega=0.05$ a.u., and $\tau=1005$ a.u. (eight complete cycles).

factor depends only on the absolute value of the momentum of the electron and not on the emission angle relative to the polarization direction. On the other hand, the argument of the hypergeometric function ${}_1F_1$, $ikr(1-\cos\theta)$, depends on the emission angle. Therefore, incorporating the hypergeometric function ${}_1F_1$ of the Coulomb wave without the normalization factor [Fig. 2(b)] yields an emission spectrum more closely resembling the exact pattern $|Y_2^0(\theta)|^2$. In view of the subtle effects the different pieces of the Coulomb wave functions have on the two-dimensional (2D) momentum distribution, it is instructive to inquire into the corresponding result for the EVA [Eq. (12)]. In the eikonal limit of the Coulomb function both the normalization factor and the ${}_1F_1$ have disappeared and are replaced by a θ-dependent rapidly oscillating phase factor [11]. The resulting 2D emission pattern [Fig. 2(c)] resembles that of the TDSE [Fig. 1(c)]. However, even though the eikonal wave function has the same asymptotic behavior as the full Coulomb function of Eq. (7) at large distances, the eikonal approximation underestimates the absolute emission probability of slow electrons by several orders of magnitude. The success of the CVA is therefore due to the correct behavior of the wave function at both small and large distances r from the nucleus.

For smaller Keldysh parameters, ionization proceeds by barrier tunneling or even above-barrier transitions rather than by multiphoton absorptions [42]. In Fig. 3 we present results for an eight-cycle ($\tau=1005$ a.u.) laser field with a peak amplitude $F_0=0.0377$ a.u. and a laser frequency $\omega=0.05$ a.u., which corresponds to a Keldysh parameter $\gamma=1.33$ in the transition from multiphoton to the tunneling regime. The intensity of the ATI rings visible in both the SFA and the CVA approximations [Figs. 3(a) and 3(b)] decrease much more rapidly with increasing energy than the exact result. While the SFA and CVA predict a decrease by approximately two orders of magnitudes between the first and fifth ATI rings [Figs. 3(a) and 3(b)], the exact distribution exhibits such a

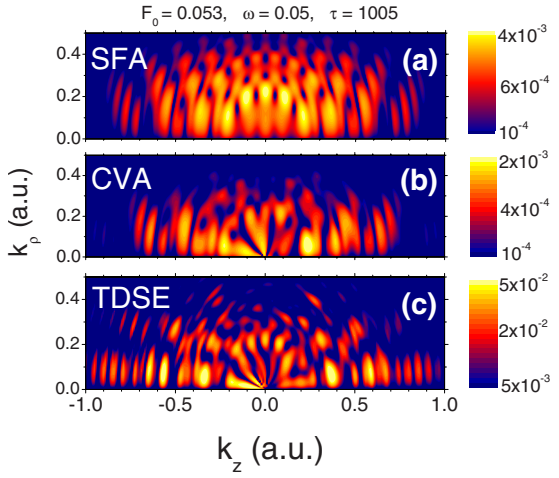

FIG. 4. (Color online) As Fig. 3 but with peak electric field F_0=0.0533 a.u.

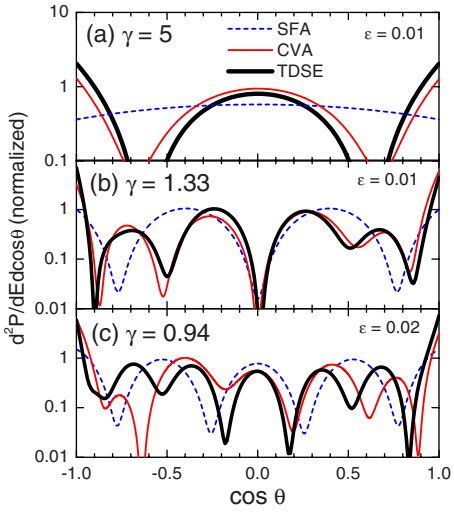

FIG. 5. (Color online) Normalized doubly-differential momentum distribution as a function of the cosine of the ejection angle of the electron for a fixed energy ε and different laser parameters: (a) F_0=0.05 a.u., ω=0.25 a.u., and τ=151 a.u., (b) F_0=0.0377 a.u., ω=0.05 a.u., and τ=1005 a.u., and (c) F_0=0.053 a.u., ω=0.05 a.u., and τ=1005 a.u.. The corresponding Keldysh parameters are indicated in the figures. (Blue) Dashed line, SFA; (red) solid line, CVA; (black) thick solid line, exact *ab initio* results.

decrease only between the first and the ninth ATI rings [Fig. 3(c)]. This discrepancy is due to the neglect of rescattering and resonance processes in both distorted-wave approximations [43]. Another remarkable feature is the differences in fringes or nodal line patterns. The SFA predicts a vertical fringe pattern for the doubly-differential momentum distribution [31]. In particular, the first ring consists of four symmetric stripes with a minimum at k_z=0. In turn, the CVA shows very clearly the bouquet-shape structure inside the first ring, resembling exact calculations of Fig. 3(c). As the Keldysh parameter is further decreased (γ=0.94 in Fig. 4), the same qualitative trends are visible, however, the quantitative agreement between the CVA and the exact result deteriorates.

A closer inspection of the normalized angular distribution inside the first ATI ring (Fig. 5) at a fixed energy reveals remarkable differences as a function of the Keldysh parameter. In Fig. 5(a), for the same laser parameters as in Fig. 1, γ=5, the CVA closely reproduces the angular distribution of the exact result while the SFA yields a different almost structureless distribution. In Fig. 5(b) (γ=1.33, same parameters as Fig. 3), the SFA predicts three minima while the CVA predicts a total number of five minima in agreement with the exact results. With decreasing γ, the agreement between the CVA and the exact result deteriorates. In Fig. 5(c), where the peak amplitude is increased up to F_0=0.0533 a.u., and consequently the Keldysh parameter lowers up to γ=0.94, the number of minima predicted by the CVA is six in agreement with the exact angular distribution. However, the positions of the minima and maxima do not coincide. Possible reasons include the neglect of rescattering and depletion of the ground state as well as excited intermediate states.

It is instructive to analyze the angular distributions of Fig. 5 in terms of path interference [17]. Within the SFA, the Coulomb potential of the remaining core after electron emission is completely neglected. Consequently, the path interference built into this description is that of photodetachment of short-range potentials, i.e., negative ions (e.g., H^-), where electrons recede on straight lines. For that case, it is well known that the interference of electron emission reduces to interference from two laser-induced point sources, resembling the two-slit Young experiment [18–21]. In Fig. 5(a) the doubly-differential momentum distribution of the SFA shows a maximum at cos θ=0 (perpendicular direction) as the two-slit interference picture would predict. The angular photoemission of electrons from negative ions near threshold features a maximum (minimum) in the direction perpendicular to the polarization axis, when the minimum number of photons required to reach the continuum (n) plus the angular momentum of the ground state, $n+l$, is even (odd) [18–21]. For the case of Fig. 1, since a total of n=2 photons are needed to reach the continuum and the angular momentum of the initial state l=0, then $n+l$=2 is even, consequently, a central spot in the first ring of Fig. 1(a) is observed. An analogous behavior is also observed in Figs. 3(a) and 4(a), where the minimum numbers of photons to reach the continuum are 13 and 16, respectively [18–21,44]. By contrast, in the CVA the electron propagates in the combined Coulomb and laser fields giving rise to path interferences between different asymptotic Kepler orbits [17].

B. Formation of the cusp in the transverse electron momentum spectra

Classical trajectory simulations show that the attraction of the released electron by the remaining core, also called Coulomb focusing, is responsible for the formation of the cusp at origin in the transverse momentum distribution [14]. In Fig. 6 three examples of the normalized transverse momentum distribution are compared with exact calculations for the laser parameters of Fig. 5. In all the cases, the SFA fails to reproduce the cusp whereas the CVA does predict the cusp at $k_\perp$=0 ($\perp$=x or y), resembling the experiments [25]. Despite the qualitative success of the CVA results, the quantitative

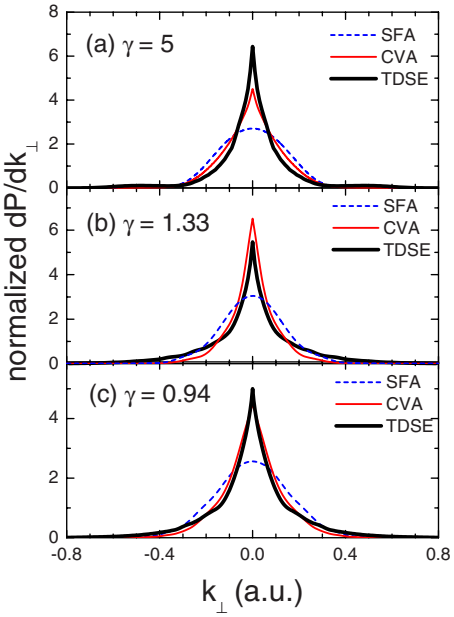

FIG. 6. (Color online) Normalized transversal momentum distributions $dP/dk_{\perp}$. (Blue) Dashed line, SFA; (red) solid line, CVA; black thick solid line, exact TDSE results. The parameters of the laser pulse are (a) F_0=0.05 a.u., ω=0.25 a.u., and τ=151 a.u., (b) F_0=0.0377 a.u., ω=0.05 a.u., and τ=1005 a.u., and (c) F_0 =0.053 a.u., ω=0.05 a.u., and τ=1005 a.u. The corresponding Keldysh parameters are indicated in the figures.

agreement of the exact transverse distribution is less than perfect. Obviously, some of the differences in the 2D distribution (Figs. 3–5) leave their marks on the transverse distribution after integrating over the longitudinal distribution.

C. Asymmetry of the longitudinal momentum spectra: Carrier-envelope phase dependence

For a cosinelike pulse (ϕ_{CE}=0), the SFA yields symmetric electron momentum distributions with respect to the plane k_z=0 as given by Eq. (14) [see e.g., Fig. 4(a)]. This is at variance with the exact calculation in the transition regime $\gamma \cong 1$ [Fig. 4(c)], where this symmetry is clearly broken. The CVA also displays a nonsymmetric forward-backward distribution. Conversely, in the multiphoton regime for γ=5 (Fig. 1), the exact result shows a complete symmetric distribution, which is reproduced by the CVA.

The forward-backward asymmetry can be quantified by the asymmetry coefficient defined as [28,45]

$$A(\phi_{\mathrm{CE}}) = \frac{W_{\phi_{\mathrm{CE}}}(0^\circ) - W_{\phi_{\mathrm{CE}}}(180^\circ)}{W_{\phi_{\mathrm{CE}}}(0^\circ) + W_{\phi_{\mathrm{CE}}}(180^\circ)}, \tag{16}$$

where $W_{\phi_{\mathrm{CE}}}(\theta) = dP/d\cos\theta = 2\pi\int_0^\infty k^2 \left(\frac{dP(\mathbf{k})}{d\mathbf{k}}\right) dk$ is the ejection probability in the $\mathbf{k}$ direction and θ is the angle subtended by

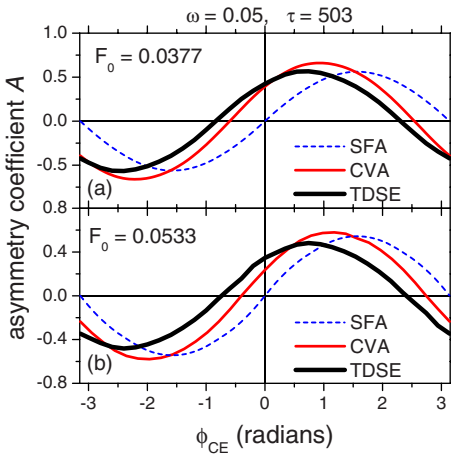

FIG. 7. (Color online) Asymmetry coefficient $A(\phi_{\mathrm{CE}})$ as a function of the carrier-envelope phase: (Blue) Dashed line, SFA; (red) solid line, CVA; and thick black line, exact TDSE results. The parameters of the field are ω=0.05 a.u., τ=503 a.u. (four complete cycles) and (a) F_0=0.0377 a.u. and (b) F_0=0.0533 a.u.

$\mathbf{k}$ and the direction of polarization $\hat{\mathbf{z}}$. For a symmetric distribution the forward (θ=0°) and backward (θ=180°) probability densities must coincide, i.e., $W(0^\circ)=W(180^\circ)$; thus, the asymmetry coefficient is zero. For an ultrashort few-cycle pulse, the asymmetry parameter depends on the carrier-envelope phase ϕ_{CE}. The ϕ_{CE} dependence of A can be used, in turn, to determine ϕ_{CE} provided the functional dependence of Eq. (16) on laser parameters is well understood.

In Fig. 7 the asymmetry coefficient is presented as a function of ϕ_{CE} for a four-cycle pulse of frequency ω=0.05 and two different field amplitudes; (a) F_0=0.0377 and (b) F_0 =0.0533. In line with the above symmetry analysis, the SFA predicts $A^{\mathrm{SFA}}(\phi_{\mathrm{CE}})=A_0^{\mathrm{SFA}}\sin(\phi_{\mathrm{CE}})$, while the exact as well as the CVA results give a shift, $A^j(\phi_{\mathrm{CE}})=A_0^j\sin(\phi_{\mathrm{CE}}+\phi_j)$, where $\phi_j>0$ for both j=CVA and TDSE. The value of A within the CVA at ϕ_{CE}=0 is $A^{\mathrm{CVA}}(\phi_{\mathrm{CE}}=0)$=0.39 and 0.24 for Figs. 7(a) and 7(b) while the TDSE results are $A^{\mathrm{TDSE}}(\phi_{\mathrm{CE}}=0)$=0.42 and 0.35, respectively. Overall, the CVA is in reasonable agreement with the TDSE results although quantitative deviations exist, indicating that the final-state Coulomb distortion accounts for a considerable portion of the asymmetry. Other sources that are neglected in the CVA should be considered as well. They include the depletion of the ground state and the contribution of excited bound states in the ionization process.

IV. CONCLUSIONS

In conclusion, we have shown that the Coulomb-Volkov approximation for photoemission by ultrashort laser pulses is capable to qualitatively, and in part even quantitatively, reproduce the two-dimensional electron momentum distribution near threshold. By contrast, we find the strong-field approximation fails to predict the bouquet-type radial pattern, in agreement to previous results by Chen *et al.* [24]. This failure is due to the neglect of the final-state Coulomb interaction. Conversely, photodetachment of negative ions with

short-ranged final state interaction should be well described by the SFA. The CVA is shown to provide a considerably improved description in comparison with SFA results in the multiphoton ($\gamma \gg 1$) and the transition from multiphoton to tunneling ($\gamma \simeq 1$) regimes. We have explicitly demonstrated this improvement for (i) the near-threshold doubly-differential momentum distributions, (ii) the formation of the cusp in the transverse momentum distribution, and (iii) the forward-backward asymmetry in the longitudinal distribution when comparing with TDSE calculations and experiments.

Future directions for applications and extensions are multielectron processes. It would be highly desirable to extend this approximation to include the rescattering process, either on a perturbative level [46] or within a distorted-wave formulation.

ACKNOWLEDGMENTS

This work was performed with financial support of CONICET, UBACyT, ANPCyT of Argentina, Hungarian-Argentine collaboration Contract No. PA05-EIII/007, by the SFB 016 ADLIS, FWF (Austria) Contract No. P15025-N08, and EU Contracts Nos. HPRI-2001-50036 and HPRI-CT-2005-026015. One of the authors (K.S.) acknowledges support by the IMRS program of the MPQ (Germany).

[1] G. G. Paulus, W. Nicklich, H. Xu, P. Lambropoulos, and H. Walther, Nature (London) **414**, 182 (2001); T. Brabec and F. Krausz, Rev. Mod. Phys. **72**, 545 (2000).
[2] G. G. Paulus, W. Nicklich, H. Xu, P. Lambropoulos, and H. Walther, Phys. Rev. Lett. **72**, 2851 (1994); G. G. Paulus *et al.*, J. Phys. B **29**, L249 (1996).
[3] R. Moshammer *et al.*, Phys. Rev. Lett. **91**, 113002 (2003); R. Wiehle, B. Witzel, H. Helm, and E. Cormier, Phys. Rev. A **67**, 063405 (2003); J. Chen and C. H. Nam, *ibid.* **66**, 053415 (2002); J. Chen, J. Liu, L. B. Fu, and W. M. Zheng, *ibid.* **63**, 011404(R) (2000).
[4] S. Dionissopoulou, T. Mercouris, A. Lyras, and C. A. Nicolaides, Phys. Rev. A **55**, 4397 (1997).
[5] X.-M. Tong and S. I. Chu, Chem. Phys. **217**, 119 (1997).
[6] N. B. Delone and V. P. Krainov, J. Opt. Soc. Am. B **8**, 1207 (1991).
[7] Gerd van de Sand and Jan M. Rost, Phys. Rev. A **62**, 053403 (2000).
[8] D. B. Milosevic, G. G. Paulus, and W. Becker, Opt. Express **11**, 1418 (2003).
[9] P. A. Macri, J. E. Miraglia, and M. S. Gravielle, J. Opt. Soc. Am. B **20**, 1801 (2003).
[10] V. D. Rodriguez, E. Cormier, and R. Gayet, Phys. Rev. A **69**, 053402 (2004).
[11] F. H. M. Faisal and J. Schlegel, J. Phys. B **38**, L223 (2005).
[12] M. Lewenstein, K. C. Kulander, K. J. Schafer, and P. H. Bucksbaum, Phys. Rev. A **51**, 1495 (1995); M. Lewenstein, Ph. Balcou, M. Yu. Ivanov, Anne L'Huillier, and P. B. Corkum, *ibid.* **49**, 2117 (1994).
[13] J. S. Cohen, Phys. Rev. A **64**, 043412 (2001); **68**, 033409 (2003).
[14] K. I. Dimitriou, D. G. Arbó, S. Yoshida, E. Persson, and J. Burgdörfer, Phys. Rev. A **70**, 061401(R) (2004).
[15] A. Rudenko *et al.*, J. Phys. B **37**, L407 (2004).
[16] C. M. Maharjan, A. S. Alnaser, I. Litvinyuk, P. Ranitovic, and C. L. Cocke, J. Phys. B **39**, 1955 (2006).
[17] D. G. Arbó, S. Yoshida, E. Persson, K. I. Dimitriou, and J. Burgdörfer, Phys. Rev. Lett. **96**, 143003 (2006).
[18] K. Krajewska, I. Ilya Fabrikant, and Anthony F. Starace, Phys. Rev. A **74**, 053407 (2006).
[19] G. F. Gribakin and M. Yu. Kuchiev, Phys. Rev. A **55**, 3760 (1997).
[20] Rainer Reichle, Igor Yu Kiyan, and Hanspeter Helm, J. Mod. Opt. **50**, 461 (2003).
[21] Rainer Reichle, Hanspeter Helm, and Igor Yu Kiyan, Phys. Rev. A **68**, 063404 (2003).
[22] Th. Weber *et al.*, Phys. Rev. Lett. **84**, 443 (2000); R. Moshammer *et al.*, *ibid.* **84**, 447 (2000).
[23] N. B. Delone and V. P. Krainov, J. Opt. Soc. Am. B **8**, 1207 (1991).
[24] Z. Chen, T. Morishita, A.-T. Le, M. Wickenhauser, X. M. Tong, and C. D. Lin, Phys. Rev. A **74**, 053405 (2006).
[25] A. Rudenko *et al.*, J. Phys. B **38**, L191 (2005).
[26] G. G. Paulus, F. Lindner, H. Walther, A. Baltuška, E. Goulielmakis, M. Lezius, and F. Krausz, Phys. Rev. Lett. **91**, 253004 (2003).
[27] S. P. Goreslavski, G. G. Paulus, S. V. Popruzhenko, and N. I. Shvetsov-Shilovski, Phys. Rev. Lett. **93**, 233002 (2004).
[28] S. Chelkowski and A. D. Bandrauk, Phys. Rev. A **71**, 053815 (2005).
[29] X. M. Tong, K. Hino, and N. Toshima, Phys. Rev. A **74**, 031405(R) (2006).
[30] J. Zhang and T. Nakajima, Phys. Rev. A **75**, 043403 (2007).
[31] M. Wickenhauser, X. M. Tong, D. G. Arbó, J. Burgdörfer, and C. D. Lin, Phys. Rev. A **74**, 041402(R) (2006).
[32] A. Becker, L. Plaja, P. Moreno, M. Nurhuda, and F. H. M. Faisal, Phys. Rev. A **64**, 023408 (2001).
[33] L. V. Keldysh, Sov. Phys. JETP **20**, 1307 (1965); F. H. M. Faisal, J. Phys. B **6**, L89 (1973); H. R. Reiss, Phys. Rev. A **22**, 1786 (1980).
[34] G. Duchateau, E. Cormier, and R. Gayet, Eur. Phys. J. D **11**, 191 (2000); G. Duchateau, E. Cormier, H. Bachau, and R. Gayet, Phys. Rev. A **63**, 053411 (2001).
[35] D. P. Dewangan and J. Eichler, Phys. Rep. **247**, 59 (1994).
[36] D. M. Wolkov, Z. Phys. **94**, 250 (1935).
[37] M. Jain and N. Tzoar, Phys. Rev. A **18**, 538 (1978).
[38] I. Cheshire, Proc. Phys. Soc. **84**, 89 (1964).
[39] L. Vainstein, L. Presnyakov, and I. Sobelman, Sov. Phys. JETP **18**, 1383 (1964).
[40] A. Messiah, *Quantum Mechanics 1* (North-Holland, New York, 1965); O. Schöller *et al.*, J. Phys. B **19**, 2505 (1986).
[41] O. Schöller, J. S. Briggs, and R. M. Dreizler, J. Phys. B **19**, 2505 (1986).
[42] For clarity, we mention that the threshold field of hydrogen,

from which the static potential barrier lowers below the initial state energy, is $F_0=0.0625$ a.u.

[43] J. Wassaf, V. Veniard, R. Taieb, and A. Maquet, Phys. Rev. A **67**, 053405 (2003).

[44] A. de Bohan, Ph.D. thesis, Université Catholique de Louvain, 2001.

[45] D. B. Milosevic, G. G. Paulus, D. Bauer, and W. Becker, J. Phys. B **39**, R203 (2006).

[46] D. Bauer, D. B. Milosevic, and W. Becker, J. Mod. Opt. **53**, 135 (2006).